Mechanistic distinctions between CHK1 and WEE1 inhibition guide the scheduling of triple therapy with gemcitabine

AUTHORS AND AFFILIATIONS

Siang-Boon Koh[1,2,3*], Yann Wallez[1], Charles R Dunlop[1], Sandra Bernaldo de Quirós Fernández[1], Tashinga E Bapiro[1,4], Frances M Richards[1] and Duncan I Jodrell[1]

[1] Cancer Research UK Cambridge Institute, University of Cambridge, Cambridge, CB2 0RE, UK

[2] Massachusetts General Hospital Cancer Center, Boston, MA 02114, USA

[3] Harvard Medical School, Boston, MA 02115, USA

[4] Oncology, IMED Biotech Unit, AstraZeneca, Cambridge, UK

*Correspondence: Siang-Boon Koh
MGH Cancer Center,
185 Cambridge Street, CPZN 4100,
Boston, MA 02114
Email: siangboon.koh@cantab.net

RUNNING TITLE: Mechanism-led DDR-based combination

KEYWORDS: CHK1, DNA damage response, drug combination, gemcitabine, WEE1

FUNDING: This work was financed by Cancer Research UK (C14303/A17197) and the Pancreatic Cancer UK Future Research Leaders fund.

CONFLICT OF INTEREST: The authors declare no potential conflicts of interest.

ABSTRACT

Combination of cytotoxic therapy with emerging DNA damage response inhibitors (DDRi) has been limited by tolerability issues. However, the goal of most combination trials has been to administer DDRi with standard-of-care doses of chemotherapy. We hypothesised that mechanism-guided treatment scheduling could reduce the incidence of dose-limiting toxicities and enable tolerable multitherapeutic regimens. Integrative analyses of mathematical modelling and single-cell assays distinguished the synergy kinetics of WEE1i from CHK1i by potency, spatiotemporal perturbation, and mitotic effects when combined with gemcitabine. These divergent properties collectively supported a triple-agent strategy, whereby a pulse of gemcitabine and CHK1i followed by WEE1i durably suppressed tumour cell growth. In xenografts, CHK1i exaggerated replication stress without mitotic CDK hyperactivation, enriching a geminin-positive subpopulation and intratumoral gemcitabine metabolite. Without overt toxicity, addition of WEE1i to low-dose gemcitabine and CHK1i was most effective in tumour control compared to single and double agents. Overall, our work provides quantitative insights into the mechanisms of DDRi chemosensitisation, leading to the rational development of a tolerable multitherapeutic regimen.

INTRODUCTION

Cancer cells contend with challenging intracellular stress arising from dysfunctional cell cycle regulations (1). In many tumour subtypes, defects in the p53 gene as well as in associated signalling pathways impair core processes of the DNA damage response (DDR) programme. This scenario renders cancer cells susceptible to exogenous damage, a concept that underpins the use of current chemotherapy. However, because of their non-selective mechanisms of action, many cytotoxic agents operate within a narrow therapeutic window. A strategy to redress this clinical issue is through the development of targeted agents that exploit cancer-specific cell cycle functions (2).

The cell cycle is regulated by a network of diverse, partly overlapping and in some cases redundant checkpoints. These fidelity-monitoring checkpoints are invoked upon DNA damage to promote cell cycle delay and DNA repair. In human cells, the G2-M checkpoint governs mitotic entry, a transition highly dependent on CDK1. A major negative regulator of CDK1 is WEE1 kinase. Under physiological condition, WEE1 activity rises during S and G2 phases in tandem with its protein expression (3). At mitotic onset, WEE1 is inhibited by CDK1 in a double-negative feedback loop to allow for the activation of the latter. Conversely, during genomic crisis, WEE1 phosphorylates CDK1 at its inhibitory residue tyrosine 15, deactivating it and thereby preventing mitotic entry (4). Apart from its involvement in G2-M transition, more recent studies have begun to clarify the functions of WEE1 during S phase. Similar to CHK1, another CDK-regulating kinase downstream of the ATR and ATM kinases, WEE1 is found to regulate DNA replication initiation and nucleotide consumption (5).

Given its multiple roles in the DDR programme, targeting WEE1 in cancer has attracted much attention. Numerous studies have now shown that WEE1i augments the effect of DNA-damaging agents, notably gemcitabine (6,7). Owing to the functional overlap between WEE1 and CHK1, the current mechanistic paradigm prescribes that WEE1i interacts with gemcitabine similarly as CHK1i does. The presumption is that both types of inhibition amplify gemcitabine-induced damage via G2-M abrogation, causing premature mitosis, mitotic catastrophe and consequently cell death (8,9). Emerging evidence has also associated WEE1i to aberrant origin firing and nucleotide depletion, culminating in phenotypes of replication stress reminiscent of those observed when ATR/CHK1 signalling is interrupted (10–13). Despite these conceptual advances, several key questions persist. There is considerable ambiguity as to whether WEE1 and CHK1 have distinct modulatory effects on the cell cycle, given that co-inhibition of the two kinases in the absence of a cytotoxic agent yields synergistic effects (14,15). It is not without precedent that kinases acting along the same pathway could have independent molecular cross-talks that lead to different outcomes when their activity is inhibited. For instance, although ATR and CHK1 both coordinate S-phase regulation, suppression of ATR triggers a DNA-PK-mediated pathway that reactivates CHK1, but such compensation is abolished when CHK1 itself is inhibited (16). Moreover, while it is evident that WEE1i and CHK1i perturb both S and G2-M checkpoints, the extent of these disruptions and how each of them contributes to chemosensitisation remain undefined.

The paucity of mechanistic insights into WEE1i and CHK1i chemosensitisation has precluded the optimal administration of these inhibitors, even though multiple WEE1i-

and CHK1i-based human trials are already underway. Indeed, earlier drug development effort has seen attrition of CHK1/2i following unacceptable toxicities in patients (17,18). The underlying cause of failure has been attributed to off-target effects than to class specificity, suggesting that tolerability issues to these inhibitors are likely to be related to dose and agent selectivity (19). In the setting of combinations, the challenge of dose-limiting toxicities becomes more prominent. When combined with chemotherapy, WEE1i multiple-dose regimen was more likely to induce toxicities in patients than WEE1i single-dose regimen (20). Likewise, gemcitabine plus CHK1i increased the frequency and severity of adverse effects in patients beyond what would be anticipated with gemcitabine alone (21). Previous work by us and others have shown that the combination of gemcitabine and CHK1i could be synergistic at low doses (11,22). This proposition has now been reinforced by early data demonstrating durable patient response following treatment of CHK1i and gemcitabine at a dose that was several times lower than the standard (23). Nevertheless, it remains debatable how these kinase inhibitors should be deployed as combinations. Based on earlier studies that presuppose G2-M abrogation as the mechanism of chemosensitisation, CHK1i and WEE1i are to be given sequentially after and not concurrently with DNA-damaging agents (24,25). Many trials have adopted similar approaches of staggered administration, but the outcome for CHK1i thus far has been modest at most (26,27). Taken together, there is a need to establish optimal dosing schedules for these agents before they could be confidently inducted into the clinic.

We hypothesised that a mechanism-based approach to optimising the doses and schedules of cell cycle checkpoint inhibitors with chemotherapy could facilitate the

development of more tolerable and effective multitherapeutic strategies. To this end, we sought to build a comparative mechanistic framework of WEE1i and CHK1i in the context of gemcitabine sensitisation. Because gemcitabine is a major component of the standard treatment for pancreatic ductal adenocarcinoma, against which few targeted agents have been successfully used, we focused our investigation on preclinical models of pancreatic cancer. Through the concerted application of mathematical modelling and single-cell analyses, our effort uncovered important distinctions in cell cycle kinetics between WEE1i and CHK1i, leading to the rational implementation of a triple-agent schedule capable of inducing cancer-specific lethality at minimally bioactive single-agent doses.

MATERIALS AND METHODS

Cell lines and chemicals

All human pancreatic ductal adenocarcinoma lines were obtained from either the European Collection of Cell Cultures or the American Type Culture Collection, authenticated using either Promega GenePrint10 system or Promega PowerPlex 16HS kit. MIA PaCa-2 FastFUCCI cell line was generated as previously described (28). Murine pancreatic ductal adenocarcinoma lines DT8082 and K8484 were established from $KRas^{G12D}$ $p53^{R172H}$ Pdx1-Cre mice. All cell lines were routinely verified to be mycoplasma-free using the Mycoprobe Mycoplasma Detection Kit (R&D Systems); the most recent date of testing was 30 January 2018. All cell lines were used within 20 passages following thawing in all experiments. 5-bromo-2'-deoxyuridine (BrdU, Sigma), CHIR124 (Selleck Chemicals), gemcitabine (Tocris), MK1775 (Selleck Chemicals), MK8776 (Selleck Chemicals) and roscovitine (Sigma) were dissolved in dimethylsulphoxide (DMSO, Sigma) in aliquots of 10-30 mM as stocks. Final DMSO concentrations were kept constant (≤0.2%) in all experiments.

Cytotoxicity and clonogenic assays

For cytotoxicity assays, cells were seeded in 96-well black-walled plates. After 24 hours, cells were treated with a serial dilution of specified agents in an 8X8 concentration format, with an extra plate fixed at the time of dosing to determine the T0 value. After specified days, cells were fixed with trichloroacetic acid and stained with sulforhodamine B. Fluorescent readout was evaluated using the Infinite 200 PRO microplate reader (Tecan) at excitation and emission wavelengths of 488 nm and 585 nm, respectively. The T0 value was subtracted from all wells, and growth inhibition was calculated by

expressing it as a ratio of the mean of vehicle control wells. Synergy score was determined as previously described (11). For clonogenic assays, equal number of viable cells were plated 24 hours prior to treatment. After the specified treatment schedule, cells were fixed with 70% methanol and stained with 0.2% crystal violet (Sigma). Colonies were imaged and quantified using GelCount colony counter (Oxford Optronix).

IncuCyte time-lapse imaging

Images were taken with the IncuCyte Live Cell Imaging microscopy (Essen Bioscience) at every three hours under cell culture conditions with 10-20X objective. Cell confluence was averaged from multiple fields of view per well. Relative confluence values were calculated by normalising each value to the time zero (T0) value.

Quantitative fluorescence-based microscopy

Images of fluorescently labelled samples were acquired using the iCys laser scanning cytometer (CompuCyte) (40X objective) equipped with a motorised Olympus IX71 inverted fluorescence microscope, three lasers (405 nm violet diode laser, 488 nm argon laser, 633 nm helium-neon laser) and three optical filter sets (blue 450/40, green 530/30, far-red 650LP) coupled to photomultiplier (PMT). The in-built iCys software was used to analyse the acquired images. Overlap-proportional Venn diagrams were drawn with the Venn diagram plotter software from Pacific Northwest National Laboratory (http://omics.pnl.gov/).

FastFUCCI imaging

The FastFUCCI live-cell assay was performed as previously described (28). Briefly, cells were seeded in glass bottom chamber (ibidi GmbH) and were kept under cell culture conditions. Images were retrieved using a Nikon Eclipse TE2000-E microscope

with a 20X long-working distance dry objective and a sCMOS Andor Neo camera. Red and green fluorescence were acquired using a pE-300white CoolLED source of light filtered by Nikon FITC B-2E/C and TRITC G-2E/C filter cubes, respectively. Live-cell time-lapse sequences were split into single channel sequences, and were applied with background subtraction and shading correction. Cell-tracking analysis was performed using the TrackMate plug-in available in the Fiji package.

Immunostaining and immunoblotting

For immunostaining, cells seeded in glass bottom chamber (ibidi GmbH) were fixed with 4% paraformaldehyde, stained with antibodies and counterstained with 4',6-diamidino-2-phenylindole (DAPI). 5-ethynyl-2'-deoxyuridine (EdU) Click-it assay was performed according to manufacturer's instructions (Life Technologies). For immunoblotting, whole-cell extracts were lysed using radioimmunoprecipitation assay (RIPA) buffer (50 mM Tris pH8, 2 mM EDTA, 150 mM sodium chloride, 1% NP-40, 0.5% sodium deoxycholate, 0.1% sodium dodecyl sulfate). Protein concentrations were quantified by the Bio-Rad Protein Assay (Bio-Rad). Equal amounts of protein were resolved using the SDS-PAGE gel system (Life Technologies) and transferred to nitrocellulose membranes using the iBlot Dry Blotting System (Thermo Fisher Scientific). Blots were blocked with Odyssey blocking buffer (LICOR), stained with primary and secondary antibodies, and analysed using the Odyssey Infrared Imaging System (LICOR).

Antibodies

Primary antibodies used were from Cell Signalling unless otherwise mentioned: β-actin (Abcam #ab6276), BrdU (BD Pharmingen #555627), cleaved caspase 3 (#9664), CDK1 (Abcam #ab18), CDK1 Y15 (#9111), CHK1 (#2360), CHK1 S296 (#2349), CHK1 S345

(#2348), ENT1 (Abcam #ab135756), H2AX (#7631), H2AX S139 (Millipore #05-636), H3 (#9715) and H3 S10 (#3377). For secondary antibodies, Alexa 488 (#4408, #4412) and Alexa 647 (#4410, #4414) from Cell Signalling were used in immunostaining. IRDye800-conjugated (#925-32210, #926-33210) and IR680-conjugated (#926-68070, #926-68021) antibodies from LICOR were used in immunoblotting.

Mouse studies

All mouse experiments were carried out in the CRUK Cambridge Institute Biological Resources Unit, in accordance with the UK Animals (Scientific Procedures) Act 1986, with approval from the CRUK Cambridge Institute Animal Ethical Review and Welfare Body. Subcutaneous xenografts of MIA PaCa-2 cells were conceived by implanting $5X10^6$ cells in 50% Matrigel/50% PBS, in the right flank of 6-10 weeks' old female BALB/c nude mice (Charles River Laboratories). For efficacy study, mice with established tumour (~300 mm^3) were randomised into three per group and treated accordingly. Gemcitabine (LKT Laboratories) and MK8776 (Selleck Chemicals) were co-dissolved in 20% hydroxypropyl-β-cyclodextrin (Vehicle I, Sigma) and were given to mice at 50 mg/kg intraperitoneally. MK1775 (Selleck Chemicals) was dissolved in 0.5% methylcellulose (Vehicle II, Sigma) and were given to mice at 60 mg/kg by oral gavage. For each weekly cycle in the efficacy study, Vehicle I or agents (gemcitabine, MK8776) were given first followed 4 hours later by Vehicle II or MK1775, on Day 0 and Day 3. Mice were killed once the averaged tumour size quadrupled (~1200 mm^3). For analysis, the normalised average of the tumour size per group during treatment phase was modelled by means of a mixed model, with treatment groups and time (polynomial of degree 2) as predictors in the fixed part of the model. The within-mouse and time

dependences were taken into account by means of random intercept and slopes as well as a moving average for the within-mouse residuals. Model checks and sensitivity analyses suggested a good model fit. Restricted maximum likelihood estimates, standard errors, as well as the degrees of freedom, t-values and p-values of the corresponding significance test for all fixed effect parameters were calculated.

Quantitative liquid chromatography-tandem mass spectrometry (LC-MS/MS)

Snap-frozen tumour tissue was homogenised in ice-cold acetonitrile (50% v/v containing tetrahydrouridine) using a Precellys 24 homogeniser (Bertin Technologies). An aliquot (50 µL) of the homogenate was transferred to a clean tube containing 150 µL of ice-cold acetonitrile (50% v/v containing internal standards CTP–$^{13}C,^{15}N_2$ from Sigma and dFdC-$^{13}C,^{15}N_2$ from Toronto Research Chemicals) followed by centrifugation at 21000 G for 20 minutes. The supernatant was transferred to a clean tube and evaporated to dryness under air. The residue was resuspended in water and 15 µL was injected into the mass spectrometer. For plasma samples, 25 µL was added to 150 µL of ice-cold acetonitrile (85% v/v containing internal standard dFdC-$^{13}C,^{15}N_2$) and the mix was processed as described for tissue homogenate. Chromatography was performed using an Accela pump (Thermo Fisher Scientific) and the analytes were separated on a PGC Hypercarb column (100 X 2.1 mm ID, 5 µm; Thermo Fisher Scientific) fitted with a guard column (Hypercarb 10 X 2.1 mm, 5 µm; Thermo Fisher Scientific) with (A) 10 mM ammonium acetate, pH10 and (B) acetonitrile as mobile phases. LC-MS/MS was performed on a TSQ Vantage triple stage quadrupole mass spectrometer (Thermo Fisher Scientific) fitted with a heated electrospray ionisation (HESI-II) probe operated in positive and

negative mode at a spray voltage of 2.5 KV, capillary temperature of 150ºC. Data acquisition was performed using LC Quan2.5.6 (Thermo Fisher Scientific).

Immunohistochemistry

Immunohistochemistry was performed on formalin-fixed, paraffin-embedded sections of tumour after heat-induced epitope retrieval by sodium citrate at 100°C for 10-20 minutes, using Bond Polymer Refine Detection kit on the automated Bond system according to manufacturer's instructions (Leica). Pre-staining dewaxing and rehydration, as well as post-staining dehydration and clearing, were performed on Leica ST5020 Multistainer. 3,3'-diaminobenzidine (DAB) enhancer (Leica) was applied to increase contrast between chromogen-specific staining and the slide background. Slides were mounted using Leica CV5030 Coverslipper Workstation and scanned using a ScanScopeXT (Aperio Technologies). Quantification was performed using the ImageScope (Aperio Technologies). Antibodies used for immunohistochemistry were geminin (Novocastra #NCL-L-GEMININ), H2AX S139 (Cell Signalling #9718) and H3 S10 (Upstate #06-570).

Statistics

Data were analysed using GraphPad Prism built-in statistical tests indicated in relevant figure legends. The following asterisk system for p value was used: *p≤0.05, **p≤0.01, ***p≤0.001, ****p≤0.0001.

RESULTS

WEE1i and CHK1i elicit chemosensitivity with different potency

In human (AsPC-1, Capan-1, HPAF-II, MIA PaCa-2, Panc-1) and murine (DT8082, K8484) pancreatic adenocarcinoma cell lines showing different cell doubling times, WEE1i (MK1775) demonstrated a ~6-fold range of single-agent sensitivity, with GI_{50} from 80±19 nM to 455±28 nM (Fig. S1A). Irrespective of the degree of sensitivity, all tested cell lines were sensitised to gemcitabine upon WEE1 inhibition (Fig. 1A, S1B-E). To analyse the data in pharmacologically meaningful terms, we used two independent mathematical models of synergy (Bliss and Loewe) to assess the combination of gemcitabine and MK1775 across a broad range of concentrations (Fig. 1A). Consistently, both models identified a synergistic interaction between the two agents. However, when we compared gemcitabine+WEE1i synergy metrics to those of gemcitabine+CHK1i (MK8776), we found that non-inhibitory concentrations ($<GI_{10}$) of CHK1i with 10-30 nM gemcitabine achieved greater synergy scores than equipotent single-agent concentrations of WEE1i (Fig. 1A). The same conclusion was reached with the use of two other structurally distinct CHK1-specific inhibitors, CHIR124 and S1181, suggesting that the differential synergism was not due to off-target effects (11). To further substantiate these findings, we tested the combinations on a more gemcitabine-resistant cell line Panc-1, again demonstrating that CHK1i elicited greater synergistic inhibition with gemcitabine than WEE1i at non-inhibitory concentrations (Fig. S1E). Crucially, at equivalent inhibitory concentration ratios (Fig. S1E), long-term clonogenic assays show similar extents of growth inhibition in both gemcitabine+WEE1i and gemcitabine+CHK1i, establishing in each instance a bona fide synergy that was durable

(Fig. 1B). Together, these data demonstrate that, while WEE1i and CHK1i induce gemcitabine hypersensitivity, there exists a disparity in synergy potential where CHK1i chemosensitises cells more effectively than WEE1i when given concurrently with gemcitabine.

WEE1i invokes two forms of DNA damage with gemcitabine

WEE1i is commonly presumed to deregulate the DNA replication apparatus in a similar manner as CHK1i. To test this notion, we exposed MIA PaCa-2 cells to the minimum synergistic concentration of WEE1i (300 nM MK1775) and CHK1i (1 μM MK8776) with 10 nM gemcitabine that elicited equivalent growth inhibition, as derived from their respective synergy metrics (Fig. 1A). Notably, these concentrations were clinically attainable and tolerable in humans (20,29,30). While gemcitabine alone induced a marginal increase in S-phase fraction, both WEE1i and CHK1i with gemcitabine caused robust S/G2 accumulation (Fig. S1F). Activation of the CDK members promotes DNA replication origin firing. Accordingly, suppression of origin firing with a broad CDK inhibitor roscovitine partially reversed growth inhibition by gemcitabine+WEE1i and gemcitabine+CHK1i (Fig. S1G) (11). However, as opposed to other deoxynucleotides, supplementation of deoxycytidine alone, which antagonises gemcitabine by competing for incorporation into DNA, was sufficient to rescue proliferation in both combinations (Fig. S1H-I). These findings indicate that, although nucleotide exhaustion induced by WEE1i and CHK1i has frequently been reported as the cause of gemcitabine sensitisation, at synergistic concentrations, increased gemcitabine incorporation following aberrant origin firing represents the predominant source of replication stress.

The differences in replication perturbation by WEE1i and CHK1i, if any, could be masked by bulk responses of cell population. To address this limitation, we turned to measuring molecular markers of genomic stress and damage in each individual cell. Exposure to gemcitabine+WEE1i and gemcitabine+CHK1i for 24 hours induced comparable levels of RPA32 S4/8 and γH2AX with few (<5%) cleaved caspase-3-positive cells, establishing a correlation between extensive replication stress (RPA32 S4/8) and apoptosis-independent DNA damage (γH2AX without substantial cleaved caspase-3) (Fig. 1C, S1J). However, while the expression of these markers was comparable in the combinations, quantitative single-cell analysis reveals that cells exposed to WEE1i alone harboured significantly higher levels of γH2AX compared to CHK1i (Fig. 1C, S1K). No difference in replication stress levels as measured by hyperphosphorylated RPA32 was found between these two conditions. Furthermore, a significantly lower fraction (54±5%) of the damaged population exposed to gemcitabine+WEE1i featured replication stress, in contrast to the 72±3% in gemcitabine+CHK1i (Fig. 1D). Together, these data suggest that the genomic damage created by WEE1i in the presence of gemcitabine could evolve from replication stress-dependent and -independent routes, raising a key question on how these effects are manifested in each phase of the cell cycle.

Passage through mitosis underlies WEE1i chemosensitisation

The above findings implied a biological consequence of WEE1 inhibition that was distinct from replication deregulation. To pursue this hypothesis, we first quantified the cell cycle durations using the live single-cell FastFUCCI assay (28). Compared to vehicle and WEE1i-only conditions, synergistic 10 nM gemcitabine+300 nM WEE1i

resulted in an increase in mean S/G2 residence time (Fig. 2A). However, the increase in S/G2 duration induced by 10 nM gemcitabine+300 nM WEE1i did not differ from that by 10 nM gemcitabine alone. In contrast, mean S/G2 duration was longer with synergistic concentrations of gemcitabine+CHK1i than with 10 nM gemcitabine (Fig. 2B). This disparity was in spite of both combinations prolonging G1 to an extent that was as much as that in high (100 nM) concentration of gemcitabine (Fig. S2A-B). Notably, both WEE1i and CHK1i partially abrogated the S/G2 prolongation induced by 100 nM gemcitabine (Fig. 2A-B), in agreement with the concentration-dependent model of G2-M abrogation (11). Together, the data reveal differential cell cycle timing effects by WEE1i and CHK1i at synergistic concentrations with gemcitabine, even though the ultimate consequence is a delay in S/G2 (Fig. S1F).

The integrity of S/G2 and mitosis are dynamically linked across cell generations (31). To systematically deconstruct this biological flux, we measured the duration of each cell cycle stage of first- and second-generation cells following gemcitabine+WEE1i. Surprisingly, despite the collective delay in S/G2 phase (Fig. 2A, S1F), the S/G2 phase of first-generation cells in the treated sample was comparable with that in control, suggesting an initial reprieve of S/G2 impediment (Fig. 2C, S2C). This observation was in contrast to CHK1i, which could prolong the S/G2 residence time as much as two folds in the first cycle (11). Upon entering mitosis, mitotic duration in the gemcitabine+WEE1i-treated cohort was more than three times longer than control (Fig. 2C, S2C). All subsequent cell cycle stages in the treated sample were also significantly protracted. To interpret these spatiotemporal details in the context of cellular responses, we tracked the fate evolution of gemcitabine+WEE1i-treated cells using three approaches. First,

quantification of individual cell fates shows that (1) the majority of non-division events in the first cycle arose during or after mitosis (47% cytokinesis failure and 33% mitotic death, compared to 20% death in S/G2), and that (2) the incidence of non-division escalated from 30% in the first cycle to 78% in the second cycle (Fig. 2D). Second, cross-generation analysis indicates that (1) 75% of second-generation cells arising from productive first-generation cells subsequently experienced a deleterious event (cytokinesis failure, cell cycle arrest, cell death), but (2) all unproductive first-generation cells (i.e. those that underwent cytokinesis failure) were again unproductive in the second cycle (Fig. S2D). Third, pairwise sister cell examination reveals that (1) a productive sister did not necessarily predict a productive counterpart, but (2) if one of the sisters was unproductive, the other sister tended to share the same fate (Fig. S2E). Together, these data demonstrate that WEE1i chemosensitisation is most profound only after a cell launches into its first mitosis, with deleterious events occurring during or after mitosis and persisting over generations.

WEE1i effects on cell cycle kinetics are temporally coordinated

Abrogation of G2-M checkpoint is frequently regarded as the mechanism of WEE1i and CHK1i, but precisely when and in which cell cycle stage the event could arise are unknown. We previously showed that CHK1i at synergistic concentrations with gemcitabine in fact did not effectively override G2-M checkpoint (11). In contrast, gemcitabine+WEE1i induced a demonstrable reduction in inactive CDK1 Y15 that correlated with an increase in mitotic marker H3 S10, suggesting CDK hyperactivation and accumulation of mitotic cells (Fig. 3A). Comparative single-cell analysis shows that the mitotic DNA content in gemcitabine+WEE1i sample was significantly lower than its

single-agent controls and CHK1i, further indicating a mitotic subset with incomplete (<4N) genome (Fig. 3B, S3A). As measured by the level of γH2AX, both WEE1i and CHK1i combinations with gemcitabine invoked comparable degrees of genomic damage in S/G2/M cells (Fig. S3B). However, quantitative immunofluorescence shows that WEE1i alone induced greater genomic damage in the mitotic fraction than CHK1i alone. This difference was particularly pronounced when WEE1i was combined with gemcitabine, where 95% of mitotic cells exhibited dramatic DNA fragmentation decorated with intense γH2AX, compared to 60% in gemcitabine+CHK1i (Fig. S3B). Collectively, these data illustrate the superiority of WEE1i over CHK1i in driving cancer cells into stressful mitotic states.

The persistent presence of a mitotic subset with normal 4N DNA under WEE1i conditions suggested that not all affected cells were compelled into mitosis directly from S phase (Fig. S3C). To resolve how WEE1i impacted the S and mitotic phases, we segregated asynchronous cell population into early, mid and late S phases as well as mitosis using quantitative multiparametric image-based cytometry. Acute WEE1 inhibition for 1 hour delayed mitotic progression but drove a fraction of only late S-phase cells into mitosis (Fig. 3C, S3D). Simultaneously, about 1 in every 3 cells in mid and late S phase compartments experienced DNA damage (Fig. 3D, S3E). Co-staining of H3 S10 and native BrdU confirms that mitotic accumulation started within 1 hour; however, it was after this timepoint that single-stranded DNA (ssDNA) became evident in the mitotic population (Fig. 3E-F, S3F). Notably, ~40-50% of <4N premature mitotic cells harboured ssDNA at 4 and 8 hours following treatment, suggesting that these cells were under-replicated and may still be replicating (Fig. S3F). Pulse labelling with EdU

indicates that there was indeed active DNA synthesis predominantly in late-S and prophase cells, in line with stress-triggered mitotic DNA replication (Fig. S3G) (32). Within the same timeframe, there was neither mitotic block nor accumulation of ssDNA-harbouring mitotic cells with CHK1 inhibition, reinforcing the notion that the mitotic consequences of CHK1i are not acute (Fig. S3H). Together, these data show three temporally coordinated but independent responses following WEE1 inhibition: (1) Upon initial insult, replication stress-independent mitotic block is enacted in mitotically competent (4N) cells. (2) Concurrently, a fraction of mid to late S-phase cells encounter genomic damage. (3) At the same time, a subset of late S-phase (<4N) cells prematurely slip into mitosis. These premature mitotic cells persist to synthesise DNA ineffectively, with WEE1i-induced CDK hyperactivation further aggravating the mitotic state by delaying its resolution.

Scheduled gemcitabine/CHK1i/WEE1i sustains tumour cell inhibition

Our data thus far show that the respective interactions of WEE1i and CHK1i with gemcitabine are synergistic but differ in several other pharmacological terms (Fig. 4A). First, although both inhibitors induce gemcitabine hypersensitivity to equal synergistic levels, CHK1i generates greater synergy at equivalent single-agent inhibitory concentrations than WEE1i (Fig. 1, S1). Second, although both inhibitors trigger replication stress, WEE1i prolongs S/G2 only after the first cell cycle, with catastrophic events occurring chiefly during or following mitosis, coincident with cross-generation damage accruement (Fig. 2, S2). Third, unlike CHK1 inhibition where mitotic distress originates from a deregulated replication checkpoint, WEE1i directly affects both mitotic entry and progression by potent disinhibition of mitotic CDK (Fig. 3, S3). From a

therapeutic perspective, these distinctions are consistent with the reported synergy between WEE1i and CHK1i (14,15). Furthermore, analysis of two cancer cell line databases shows that WEE1 and CHK1 expression were significantly correlated in diverse cancer subtypes (Fig. 4B, S4A). In agreement, cell lines with high WEE1 or CHK1 expression were more sensitive to a WEE1/CHK1 dual inhibitor 681640, but such association was less robust in a CHK1/2-specific inhibitor AZD7762, arguing from a genetic perspective the advantage of co-targeting the two kinases (Fig. S4B) (33). Importantly, the trend of a positive correlation between WEE1 and CHK1 expression was also observed in multiple patient samples of different tumour origins (Fig. S4C). In primary pancreatic ductal adenocarcinoma, high expression of these kinases was a strong determinant of poor overall survival and disease-free survival (Fig. 4C, S4D). Equally, overexpression of these kinases was associated with shorter overall survival in three other aggressive tumours, including lung adenocarcinoma where gemcitabine is also used routinely. Together, these findings offer a compelling rationale to combine WEE1i with CHK1i to maximise gemcitabine sensitivity.

To determine optimal dosing schedules for WEE1i and CHK1i with gemcitabine, we used real-time *in vitro* imaging and found that delayed administration of CHK1i at 24 hours relative to gemcitabine did not lead to substantial growth inhibition (Fig. 4D). Conversely, concurrent administration yielded dramatic growth suppression, even when gemcitabine and CHK1i were removed after 24 hours. Given that G2-M abrogation was not the predominant mechanism of synergy for gemcitabine+CHK1i, we hypothesised that the combination could be further enhanced by driving G2-M bypass using WEE1i. We determined the growth kinetics of MIA PaCa-2 cells exposed to the schedule of

gemcitabine+CHK1i (MK8776 or CHIR124) for 24 hours followed by WEE1i (Fig. 4E). Cell growth inhibition was remarkably durable with the triple regimen compared to vehicle and dual agent controls. Notably, substitution of WEE1i in the triple regimen with another CHK1i (i.e. gemcitabine+MK8776 followed by CHIR124, or gemcitabine+CHIR124 followed by MK8776) failed to recapitulate the durable response. Long-term clonogenic assays confirm effective growth suppression of the proposed triple regimen and further show that administering gemcitabine+CHK1i followed by WEE1i was more effective than administering gemcitabine+WEE1i followed by CHK1i (Fig. S4E-F). Together, the sequence-dependent cooperativity of WEE1i with gemcitabine+CHK1i validates the differential mechanistic properties of WEE1i and CHK1i, affirms the lethality of G2-M bypass, and demonstrates the antitumour potential of the proposed triple regimen.

In vivo studies show antitumour potential of minimal-dose multitherapy

To evaluate whether the *in vitro* mechanistic findings could be recapitulated *in vivo*, we chose a low dose of gemcitabine (25 mg/kg) compared to the “full” maximum tolerable dose (MTD) dose (100-150 mg/kg) administered to mice bearing MIA PaCa-2 xenografts. An intraperitoneal bolus of 25 mg/kg MK8776 increased gemcitabine-induced CHK1 S345 phosphorylation and abrogated CHK1 S296 autophosphorylation for at least the first four hours, indicating target engagement (Fig. S5A-B). These changes were accompanied by an increase in γH2AX and RPA32 S4/8 without overt CDK1 hyperactivation or H3 S10 upregulation, consistent with the lack of G2-M checkpoint bypass we previously established with CHK1i S1181 (Fig. 5A, S5B-C) (11). Quantitative immunohistochemistry further confirms high genomic damage and low

mitotic index with aberrant mitoses in the combination cohort (Fig. 5B, S5D-E). Moreover, gemcitabine+MK8776 induced an accumulation of geminin-positive cells by 8 hours, indicative of high S/G2 fraction as observed in cell lines (Fig. 5C). This accumulation was in concert with intratumoral elevation of active gemcitabine metabolite 2',2'-difluoro-2'-deoxycytidine triphosphate (dFdCTP) (Fig. 5D). MK8776 did not significantly alter the pharmacokinetics of native gemcitabine (2',2'-difluoro-2'-deoxycytidine, dFdC) in tumour and in plasma, implying that there was neither increased drug uptake in tumour nor decreased drug clearance in blood (Fig. S5F). There was also no obvious difference between both treatment arms in the expression of a major gemcitabine transporter ENT1 (Fig. S5B-C). Having determined that acute administration of low gemcitabine and MK8776 in mice induced molecular responses observed *in vitro*, we tested the efficacy of the proposed triple schedule. For stringent comparison, we employed doses and treatment frequencies that were equal to or lower than those previously established to be suboptimal in MIA PaCa-2 xenograft model, which typically exhibits marginal response even to the highest doses of gemcitabine combinations (34–37). As the *in vitro* findings predicted, the triple minimal-dose regimen was most effective in the growth suppression of established (~300 mm^3) tumours compared to single- and double-agent arms (Fig. 5E). During the treatment phase (day 0 to 26), the triple regimen was the only group that trended towards a difference from the vehicle group in terms of tumour volume ($p = 0.04$ by t-test, $p = 0.08$ by Dunnett's multiple-comparison test). Following the treatment phase, the regimen delayed tumour growth by about 10 days relative to control, before the averaged tumour size quadrupled. Importantly, there was no overt weight loss in mice treated with the triple

combination, suggesting that the regimen did not impact physiological functions at least within the period of investigation (Fig. S5G). Together, the *in vivo* data support the *in vitro* mechanistic findings and demonstrate the underappreciated feasibility of minimal-dose multitherapy in achieving tumour control.

DISCUSSION

Targeting cancer with cell cycle checkpoint inhibitors in combination with chemotherapy is conceptually attractive, but the success has thus far been largely dependent on serendipity (38,39). Here, we used a mechanism-guided approach to systematically combine classic cytotoxic agent gemcitabine with two DDR clinical candidates CHK1i and WEE1i. We first established synergy between pairs of these agents through mathematical modelling of individual dose-response curves, simultaneously identifying the concentration ratios that yielded optimal growth inhibition. From a series of single-cell studies conducted at these synergistic ratios, we uncovered distinct cell cycle kinetics between CHK1i and WEE1i, contrary to the common presumption that these inhibitors affect the cell cycle similarly. Notably, upon initial exposure, CHK1i induced S-phase deregulation in cells more readily than WEE1i, which itself had more direct inimical effects on mitosis. Based on these distinctions, we devised a minimal-dose gemcitabine/CHK1i/WEE1i triple regimen that achieved tumour control without additional toxicity.

Our work represents a preclinical proof-of-concept that MTD is not necessarily the best approach in developing multitherapeutic regimens. To date, most clinical studies use MTD as a standard for dose selection of chemotherapy. This paradigm stems from historical observations that response to cytotoxic agents often correlates with dose. Recent advances in tumour evolution have begun to question the basis of MTD, given the potential rapid expansion of resistant clones from intensive drug-induced selection (40,41). The advent of targeted therapies, which unlike cytotoxic drugs exploit cancer-specific features, has also challenged the relevance of MTD (42). In one instance, meta-

analysis of 24 clinical trials shows similar outcomes between patients treated with low- and high-dose targeted agents, with the latter cohorts having higher dropout rates due to cumulative toxicities (43). These findings were supported by another study demonstrating through computational modelling that drug concentrations lower than the MTD could be equally efficacious (44). The complexity of identifying optimal doses escalates in the context of drug combinations, where their clinical benefits are tempered by further risks of off-target effects. Evidently, drug-specific dose-response kinetics and dose-dependent drug effects are formidable challenges in the design of multitherapy, and preclinical drug development should be primed to address these considerations from the outset.

An immediate clinical impact of our study is the re-evaluation of current schedules used in human trials for CHK1i and WEE1i. We demonstrate that concurrent, not sequential, treatment of gemcitabine and CHK1i leads to better tumour cell inhibition. This inhibition is further enhanced by subsequent addition of WEE1i and not continuation of CHK1i. Our proposal is grounded on the mechanisms of synergy we identified at optimal concentration ratios (Fig. 6). Synergy between gemcitabine and CHK1i relies chiefly on the collapse of the S-phase replication checkpoint (11). Higher concentrations of either agents induce G2-M bypass as a secondary mechanism, but inherent to these scenarios is a greater risk of toxicity, as has been clinically observed (17,21). Introduction of WEE1i, which we have determined to be a much superior G2-M abrogator and mitotic stressor, expands the synergy space of the dual therapy through its complementary but independent modes of action. Because this triple regimen

rationally staggers the kinase inhibitors with all agents titrated at minimally bioactive doses, it should in principle strike a balance between therapeutic activity and tolerability. The finding that the low-dose triple regimen can indeed confer tumour suppression without acute toxicity in mice warrants further exploration. A proximate extension of this tripartite DDR model is permutations of similarly acting modalities. For instance, combinations of radiotherapy with gemcitabine and WEE1i are now entering early-phase clinical trials (45). Understanding their mechanisms at optimal dose ratios can inform decisions on doses, treatment sequences and timing of administration. Equally, the triple regimen (gemcitabine, CHK1i, WEE1i) or its variant is testable in preclinical models tailored to pursuing specific questions on tumour initiation and progression. In particular, overcoming the evolution of treatment resistance is a key aspect of invoking drug combinations. Therefore, evaluating clinic-pathologic parameters such as long-term survival, metastasis and disease relapse, as well as understanding the resurgence of resistance will be crucial to innovating more effective multitherapeutic strategies. The same tenet of rationalising multipronged regimens should apply to current treatments in the clinic. Already, gemcitabine is being replaced by gemcitabine plus nab-paclitaxel and FOLFIRINOX (folinic acid, 5-fluorouracil, irinotecan, oxaliplatin) as the standard of care for pancreatic ductal adenocarcinoma, with enthusiasm in further combining them with immunotherapy (46). There is a need to identify logical ways to induct these cocktails, and we anticipate mechanism-led preclinical studies directed at defining optimal doses and schedules to be instrumental in this endeavour. Admittedly, the scope of these translational works must also be expanded to include the physical and biological properties unique to each tumour type. For instance, the heterogeneity in drug

penetration to target sites and the diversity of the tumour microenvironments are factors that could influence treatment outcome in patients. These features can only be comprehensively addressed with further development of preclinical tools and models, as well as the integration of laboratory discoveries and clinical insights.

Computational modelling on patients has shown that, while dual therapy confers clinical benefits, patients with large disease burden require triple therapy (47). There is currently no established bioinformatic tools that can predict the interaction of more than two therapeutic agents. Our approach obviates this barrier by coupling existing synergy metrics with mechanistic reasoning anchored at a single-cell level. This effort, which weights efficacy with tolerability, is a distinct component in the emerging trend of using high-resolution cellular data for the rational design of multitherapy (48,49). The implications of these detail-driven translational studies on the next generation of drug development could be profound.

ACKNOWLEDGMENTS

We thank Cancer Research UK Cambridge Institute (CRUK-CI) Biological Resources Unit, Biorepository, Flow Cytometry, Histopathology/*in situ* Hybridisation and Light Microscopy Core Facilities for technical provision; Dominique-Laurent Couturier (CRUK-CI Bioinformatics Core Facility) for statistics advice; as well as members of the Pharmacology & Drug Development Group for discussions. We acknowledge the support from the University of Cambridge, Cancer Research UK, Hutchison Whampoa Limited and Pancreatic Cancer UK.

REFERENCES

1. López-Contreras AJ, Fernandez-Capetillo O. The ATR barrier to replication-born DNA damage. DNA Repair (Amst). 2010;9:1249–55.

2. Brown JS, O'Carrigan B, Jackson SP, Yap TA. Targeting DNA Repair in Cancer: Beyond PARP Inhibitors. Cancer Discov. 2017;7:20–37.

3. Watanabe N, Broome M, Hunter T. Regulation of the human WEE1Hu CDK tyrosine 15-kinase during the cell cycle. EMBO J. 1995;14:1878–91.

4. De Witt Hamer PC, Mir SE, Noske D, Van Noorden CJF, Würdinger T. WEE1 kinase targeting combined with DNA-damaging cancer therapy catalyzes mitotic catastrophe. Clin Cancer Res. 2011;17:4200–7.

5. Beck H, Nähse-Kumpf V, Larsen MSY, O'Hanlon KA, Patzke S, Holmberg C, et al. Cyclin-dependent kinase suppression by WEE1 kinase protects the genome through control of replication initiation and nucleotide consumption. Mol Cell Biol. 2012;32:4226–36.

6. Kausar T, Schreiber JS, Karnak D, Parsels LA, Parsels JD, Davis MA, et al. Sensitization of Pancreatic Cancers to Gemcitabine Chemoradiation by WEE1 Kinase Inhibition Depends on Homologous Recombination Repair. Neoplasia. 2015;17:757–66.

7. Rajeshkumar NV, De Oliveira E, Ottenhof N, Watters J, Brooks D, Demuth T, et al. MK-1775, a potent Wee1 inhibitor, synergizes with gemcitabine to achieve tumor regressions, selectively in p53-deficient pancreatic cancer xenografts. Clin Cancer Res. 2011;17:2799–806.

8. Aarts M, Sharpe R, Garcia-Murillas I, Gevensleben H, Hurd MS, Shumway SD, et al. Forced mitotic entry of S-phase cells as a therapeutic strategy induced by inhibition of WEE1. Cancer Discov. 2012;2:524–39.

9. Morgan MA, Parsels LA, Parsels JD, Mesiwala AK, Maybaum J, Lawrence TS. Role of checkpoint kinase 1 in preventing premature mitosis in response to gemcitabine. Cancer Res. 2005;65:6835–42.

10. Pfister SX, Markkanen E, Jiang Y, Sarkar S, Woodcock M, Orlando G, et al. Inhibiting WEE1 Selectively Kills Histone H3K36me3-Deficient Cancers by dNTP Starvation. Cancer Cell. 2015;28:557–68.

11. Koh S-B, Courtin A, Boyce RJ, Boyle RG, Richards FM, Jodrell DI. CHK1 Inhibition Synergizes with Gemcitabine Initially by Destabilizing the DNA Replication Apparatus. Cancer Res. 2015;75:3583–95.

12. Toledo LI, Altmeyer M, Rask M-B, Lukas C, Larsen DH, Povlsen LK, et al. ATR prohibits replication catastrophe by preventing global exhaustion of RPA. Cell. 2013;155:1088–103.

13. Jossé R, Martin SE, Guha R, Ormanoglu P, Pfister TD, Reaper PM, et al. ATR inhibitors VE-821 and VX-970 sensitize cancer cells to topoisomerase i inhibitors by disabling DNA replication initiation and fork elongation responses. Cancer Res. 2014;74:6968–79.

14. Magnussen GI, Emilsen E, Giller Fleten K, Engesæter B, Nähse-Kumpf V, Fjær R, et al. Combined inhibition of the cell cycle related proteins Wee1 and Chk1/2 induces synergistic anti-cancer effect in melanoma. BMC Cancer. 2015;15:462.

15. Russell MR, Levin K, Rader J, Belcastro L, Li Y, Martinez D, et al. Combination therapy targeting the Chk1 and Wee1 kinases shows therapeutic efficacy in neuroblastoma. Cancer Res. 2013;73:776–84.

16. Buisson R, Boisvert JL, Benes CH, Zou L. Distinct but Concerted Roles of ATR, DNA-PK, and Chk1 in Countering Replication Stress during S Phase. Mol Cell. 2015;59:1011–24.

17. Sausville E, Lorusso P, Carducci M, Carter J, Quinn MF, Malburg L, et al. Phase I dose-escalation study of AZD7762, a checkpoint kinase inhibitor, in combination with gemcitabine in US patients with advanced solid tumors. Cancer Chemother Pharmacol. 2014;73:539–49.

18. Dees EC, Baker SD, O'Reilly S, Rudek MA, Davidson SB, Aylesworth C, et al. A phase I and pharmacokinetic study of short infusions of UCN-01 in patients with refractory solid tumors. Clin Cancer Res. 2005;11:664–71.

19. Chen T, Stephens PA, Middleton FK, Curtin NJ. Targeting the S and G2 checkpoint to treat cancer. Drug Discov Today. 2012;17:194–202.

20. Leijen S, van Geel RMJM, Pavlick AC, Tibes R, Rosen L, Razak ARA, et al. Phase I Study Evaluating WEE1 Inhibitor AZD1775 As Monotherapy and in Combination With Gemcitabine, Cisplatin, or Carboplatin in Patients With Advanced Solid Tumors. J Clin Oncol. 2016;34:4371–80.

21. Infante JR, Hollebecque A, Postel-Vinay S, Bauer TM, Blackwood EM, Evangelista M, et al. Phase I Study of GDC-0425, a Checkpoint Kinase 1 Inhibitor, in Combination with Gemcitabine in Patients with Refractory Solid Tumors. Clin Cancer Res. 2017;23:2423–32.

22. Liu Y, Li Y, Wang X, Liu F, Gao P, Quinn MM, et al. Gemcitabine and Chk1 Inhibitor AZD7762 Synergistically Suppress the Growth of Lkb1-Deficient Lung Adenocarcinoma. Cancer Res. 2017;77:5068–76.

23. Laroche-Clary A, Lucchesi C, Rey C, Verbeke S, Bourdon A, Chaire V, et al. CHK1 Inhibition in Soft-Tissue Sarcomas: Biological and Clinical Implications. Ann Oncol. 2018;

24. Hirai H, Iwasawa Y, Okada M, Arai T, Nishibata T, Kobayashi M, et al. Small-molecule inhibition of Wee1 kinase by MK-1775 selectively sensitizes p53-deficient tumor cells to DNA-damaging agents. Mol Cancer Ther. 2009;8:2992–3000.

25. Sakurikar N, Eastman A. Will targeting Chk1 have a role in the future of cancer therapy? J Clin Oncol. 2015;33:1075–7.

26. Laquente B, Lopez-Martin J, Richards D, Illerhaus G, Chang DZ, Kim G, et al. A phase II study to evaluate LY2603618 in combination with gemcitabine in pancreatic cancer patients. BMC Cancer. 2017;17:137.

27. Webster JA, Tibes R, Morris L, Blackford AL, Litzow M, Patnaik M, et al. Randomized phase II trial of cytosine arabinoside with and without the CHK1 inhibitor MK-8776 in relapsed and refractory acute myeloid leukemia. Leukemia Research. 2017;61:108–16.

28. Koh S-B, Mascalchi P, Rodriguez E, Lin Y, Jodrell DI, Richards FM, et al. A quantitative FastFUCCI assay defines cell cycle dynamics at a single-cell level. J Cell Sci. 2017;130:512–20.

29. Daud AI, Ashworth MT, Strosberg J, Goldman JW, Mendelson D, Springett G, et al. Phase I Dose-Escalation Trial of Checkpoint Kinase 1 Inhibitor MK-8776 As Monotherapy and in Combination With Gemcitabine in Patients With Advanced Solid Tumors. JCO. 2015;33:1060–6.

30. Do K, Wilsker D, Ji J, Zlott J, Freshwater T, Kinders RJ, et al. Phase I Study of Single-Agent AZD1775 (MK-1775), a Wee1 Kinase Inhibitor, in Patients With Refractory Solid Tumors. JCO. 2015;33:3409–15.

31. S Pedersen R, Karemore G, Gudjonsson T, Rask M-B, Neumann B, Hériché J-K, et al. Profiling DNA damage response following mitotic perturbations. Nat Commun. 2016;7:13887.

32. Minocherhomji S, Ying S, Bjerregaard VA, Bursomanno S, Aleliunaite A, Wu W, et al. Replication stress activates DNA repair synthesis in mitosis. Nature. 2015;528:286–90.

33. Forbes SA, Beare D, Boutselakis H, Bamford S, Bindal N, Tate J, et al. COSMIC: somatic cancer genetics at high-resolution. Nucleic Acids Res. 2017;45:D777–83.

34. Engelke CG, Parsels LA, Qian Y, Zhang Q, Karnak D, Robertson JR, et al. Sensitization of pancreatic cancer to chemoradiation by the Chk1 inhibitor MK8776. Clin Cancer Res. 2013;19:4412–21.

35. Karnak D, Engelke CG, Parsels LA, Kausar T, Wei D, Robertson JR, et al. Combined inhibition of Wee1 and PARP1/2 for radiosensitization in pancreatic cancer. Clin Cancer Res. 2014;20:5085–96.

36. Montano R, Thompson R, Chung I, Hou H, Khan N, Eastman A. Sensitization of human cancer cells to gemcitabine by the Chk1 inhibitor MK-8776: cell cycle perturbation and impact of administration schedule in vitro and in vivo. BMC Cancer. 2013;13:604.

37. Guzi TJ, Paruch K, Dwyer MP, Labroli M, Shanahan F, Davis N, et al. Targeting the replication checkpoint using SCH 900776, a potent and functionally selective CHK1 inhibitor identified via high content screening. Mol Cancer Ther. 2011;10:591–602.

38. Chen S-H, Lahav G. Two is better than one; toward a rational design of combinatorial therapy. Curr Opin Struct Biol. 2016;41:145–50.

39. Lieu CH, Tan A-C, Leong S, Diamond JR, Eckhardt SG. From bench to bedside: lessons learned in translating preclinical studies in cancer drug development. J Natl Cancer Inst. 2013;105:1441–56.

40. Enriquez-Navas PM, Kam Y, Das T, Hassan S, Silva A, Foroutan P, et al. Exploiting evolutionary principles to prolong tumor control in preclinical models of breast cancer. Sci Transl Med. 2016;8:327ra24.

41. Enriquez-Navas PM, Wojtkowiak JW, Gatenby RA. Application of Evolutionary Principles to Cancer Therapy. Cancer Res. 2015;75:4675–80.

42. Sachs JR, Mayawala K, Gadamsetty S, Kang SP, de Alwis DP. Optimal Dosing for Targeted Therapies in Oncology: Drug Development Cases Leading by Example. Clin Cancer Res. 2016;22:1318–24.

43. Jain RK, Lee JJ, Hong D, Markman M, Gong J, Naing A, et al. Phase I oncology studies: evidence that in the era of targeted therapies patients on lower doses do not fare worse. Clin Cancer Res. 2010;16:1289–97.

44. Chakrabarti S, Michor F. Pharmacokinetics and Drug Interactions Determine Optimum Combination Strategies in Computational Models of Cancer Evolution. Cancer Res. 2017;77:3908–21.

45. Cuneo KC, Morgan MA, Davis MA, Parcels LA, Parcels J, Karnak D, et al. Wee1 Kinase Inhibitor AZD1775 Radiosensitizes Hepatocellular Carcinoma Regardless of TP53 Mutational Status Through Induction of Replication Stress. Int J Radiat Oncol Biol Phys. 2016;95:782–90.

46. Kamisawa T, Wood LD, Itoi T, Takaori K. Pancreatic cancer. Lancet. 2016;388:73–85.

47. Bozic I, Reiter JG, Allen B, Antal T, Chatterjee K, Shah P, et al. Evolutionary dynamics of cancer in response to targeted combination therapy. Elife. 2013;2:e00747.

48. Chen S-H, Forrester W, Lahav G. Schedule-dependent interaction between anticancer treatments. Science. 2016;351:1204–8.

49. Lee MJ, Ye AS, Gardino AK, Heijink AM, Sorger PK, MacBeath G, et al. Sequential application of anticancer drugs enhances cell death by rewiring apoptotic signaling networks. Cell. 2012;149:780–94.

FIGURE LEGENDS

Figure 1: WEE1i and CHK1i synergise with gemcitabine with different potency.

(A) Combination assay. MIA PaCa-2 cells were treated for 72 hours. Data were analysed with two synergy mathematical models. Combinations of 10-30 nM GEM with a pair of non-inhibitory ($<GI_{10}$) equivalent concentrations of MK1775 and MK8776 are boxed in white. Bar graph shows the mean synergy score within the boxed surface. Data are represented as mean ± SEM, n=3. A two-tailed t-test was performed, *p≤0.05.

(B) Clonogenic assay. Panc-1 cells were treated for 72 hours (30 nM GEM, 300 nM MK1775, 1 µM MK8776), and were left to grow after washout for 10 days. Data are represented as mean ± SEM, n=3. A one-way ANOVA analysis was performed, *p≤0.05, ****p≤0.0001.

(C) Quantitative immunofluorescence of MIA PaCa-2 cells treated for 24 hours (10 nM GEM, 300 nM MK1775, 1 µM MK8776). Each blue, green or red dot marks a cell positive for γH2AX, RPA32 S4/8 or both, respectively.

(D) Quantification of overlap between γH2AX (red) and RPA32 S4/8 (green) in MIA PaCa-2 cells treated for 24 hours (10 nM GEM, 300 nM MK1775, 1 µM MK8776). Percentage of γH2AX-positive cells in RPA32 S4/8-positive population is in green; percentage of RPA32 S4/8-positive cells in γH2AX-positive population is in red. Red arrowhead denotes γH2AX-positive cell; yellow arrowhead denotes γH2AX/RPA32 S4/8 double-positive cell. Data are represented as mean ± SEM, n=5. At least 2000 cells per condition per replicate were analysed. A two-tailed t-test was performed, *p≤0.05. Scale bar, 25 µm.

Figure 2: Mitotic stress underlies WEE1i cytotoxicity.

(A-B) S/G2 duration of MIA PaCa-2 FastFUCCI cells treated as indicated. At least 100 cells per condition were analysed. Data are represented as mean ± SEM. A one-way ANOVA analysis was performed, ****p≤0.0001.

(C) Cell cycle duration of MIA PaCa-2 FastFUCCI cells treated with DMSO or 10 nM GEM+300 nM MK1775. A total of 243 cells were analysed. Data are represented as mean ± SEM. A two-tailed t-test was performed, *p≤0.05, **p≤0.01, ****p≤0.0001.

(D) Percentage of MIA PaCa-2 FastFUCCI cells in the first and second cycles that underwent division or not following 10 nM GEM+300 nM MK1775. Fraction of non-dividing cells was further categorised according to cell fate. A total of 122 cells were analysed.

Figure 3: Inimical effects of WEE1i are spatiotemporally defined.

(A) Immunoblotting for MIA PaCa-2 cells treated for 24 hours. The graph shows densitometric analysis of CDK1 Y15/CDK1 or H3 S10/H3, relative to DMSO.

(B) Quantification of DNA content of mitotic MIA PaCa-2 cells treated for 24 hours (10 nM GEM, 300 nM MK1775, 1 μM MK8776). Data are represented as mean, normalised to DMSO. A one-way ANOVA analysis was performed, ****p≤0.0001.

(C) Quantification of mitotic Panc-1 cells in S phase. Cells were treated with 10 μM EdU for 45 minutes followed by 3 μM MK1775 for 1 hour. S and non-S phase cells were identified based on EdU and DNA contents. Percentage of H3 S10-positive cells is shown.

(D) Quantification of damaged Panc-1 cells in S phase, treated as in (C). Percentage of γH2AX-positive cells is shown.

(E-F) Quantification of mitotic Panc-1 cells harbouring ssDNA. Cells were grown with 10 μM BrdU for 48 hours, treated with 3 μM MK1775 and immunostained for native BrdU. In (E), the first column shows positive control, where sample was acid-denatured to confirm BrdU incorporation. Scale bar, 10 μm. In (F), percentage of mitotic cells is in black and percentage of native BrdU-positive mitotic cells (out of the respective mitotic fractions) in red. At least 2000 cells were analysed per time-point. Inset shows the total native BrdU intensity per mitotic cell. A one-way ANOVA analysis was performed, ****p≤0.0001.

Figure 4: A gemcitabine/CHK1i/WEE1i regimen enhances tumour cell suppression.

(A) Schematics of the spatiotemporal effects of WEE1i and CHK1i.

(B) Correlative analysis between WEE1 and CHK1 mRNA expression in 967 tumour cell lines from the Cancer Cell Line Encyclopedia project. Pearson correlation coefficient r and p values are indicated.

(C) Kaplan-Meier analysis of RNASeq V2 data on WEE1 or CHK1 expression and patient survival in indicated primary tumour samples. Tumours with mRNA expression Z-score +1.5 were considered as tumours with high expression. Data were sourced from the TCGA Research Network.

(D-E) Real-time growth kinetics of MIA PaCa-2 cells treated as indicated (10 nM GEM, 1 μM MK8776, 20 nM CHIR124, 300 nM MK1775). Data are represented as mean ± SEM, n=3.

Figure 5: *In vivo* studies show antitumour potential of the triple regimen.

(A) Quantification of immunoblotting of tumour samples from MIA PaCa-2 xenografts treated and harvested as indicated. Data are represented as mean ± SEM, n=3.

(B) Quantification of immunohistochemistry of tumour samples from (A). γH2AX and H3 S10 were used as marker of DNA damage and mitosis, respectively. Middle line marks the mean. A two-tailed t-test was performed, *p≤0.05.

(C) Quantification of geminin-positive cells in tumour samples from (A). Data are represented as mean ± SEM, n=3. A two-tailed t-test was performed, *p≤0.05. Scale bar, 50 µm.

(D) Pharmacokinetic profile of GEM. Tumour samples from MIA PaCa-2 xenografts treated with either 25 mg/kg GEM or 25 mg/kg GEM+MK8776 were analysed for the active metabolite of GEM (dFdCTP) at specified time-points. Area under the curve (AUC) and p values are indicated.

(E) Change in tumour volume of MIA PaCa-2 xenografts. Mice were treated as indicated for four consecutive weekly cycles. Black triangle on the x-axis denotes start of each dosing cycle. Data are represented as mean ± SEM, n=3.

Figure 6: Combination of GEM, CHK1i and WEE1i maximises synergy space.

Rationale for GEM/CHK1i/WEE1i triple combination. GEM and CHK1i at optimal non-cytotoxic concentrations enforces synergy primarily via S-phase deregulation. Complementing this combination with WEE1i expands the synergy space of GEM+CHK1i by more robust induction of G2 bypass and mitotic stress.

Figure 1

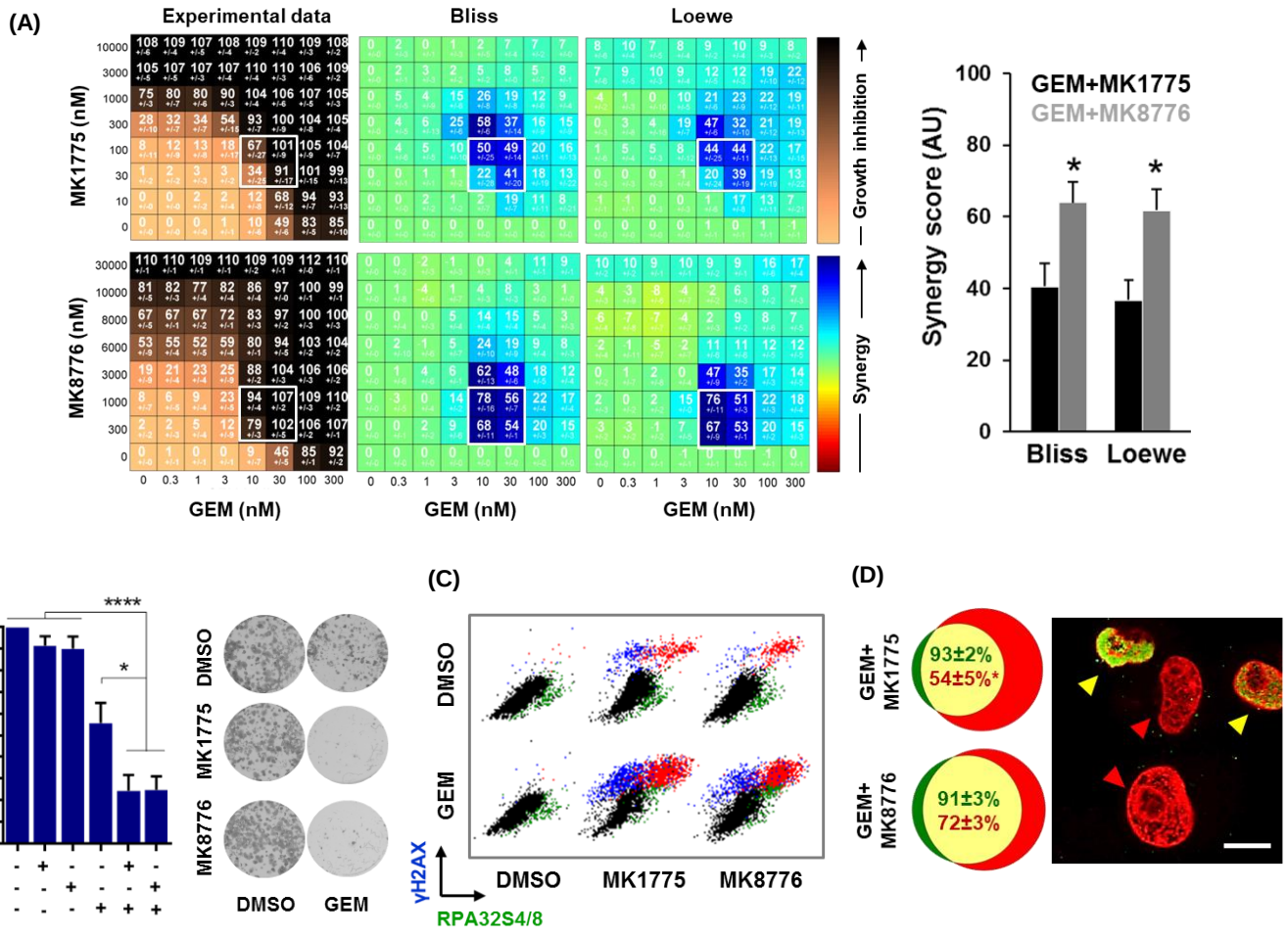
(A)
Experimental data
Bliss
Loewe
MK1775 (nM)
MK8776 (nM)
GEM (nM)
Growth inhibition
Synergy
Synergy score (AU)
GEM+MK1775
GEM+MK8776
Bliss
Loewe
(B)
Relative viable fraction (AU)
****
*
MK1775
MK8776
GEM
DMSO
(C)
DMSO
GEM
γH2AX
RPA32S4/8
MK1775
MK8776
(D)
GEM+ MK1775
93±2%
54±5%*
GEM+ MK8776
91±3%
72±3%
γH2AX RPA32 S4/8

Figure 2

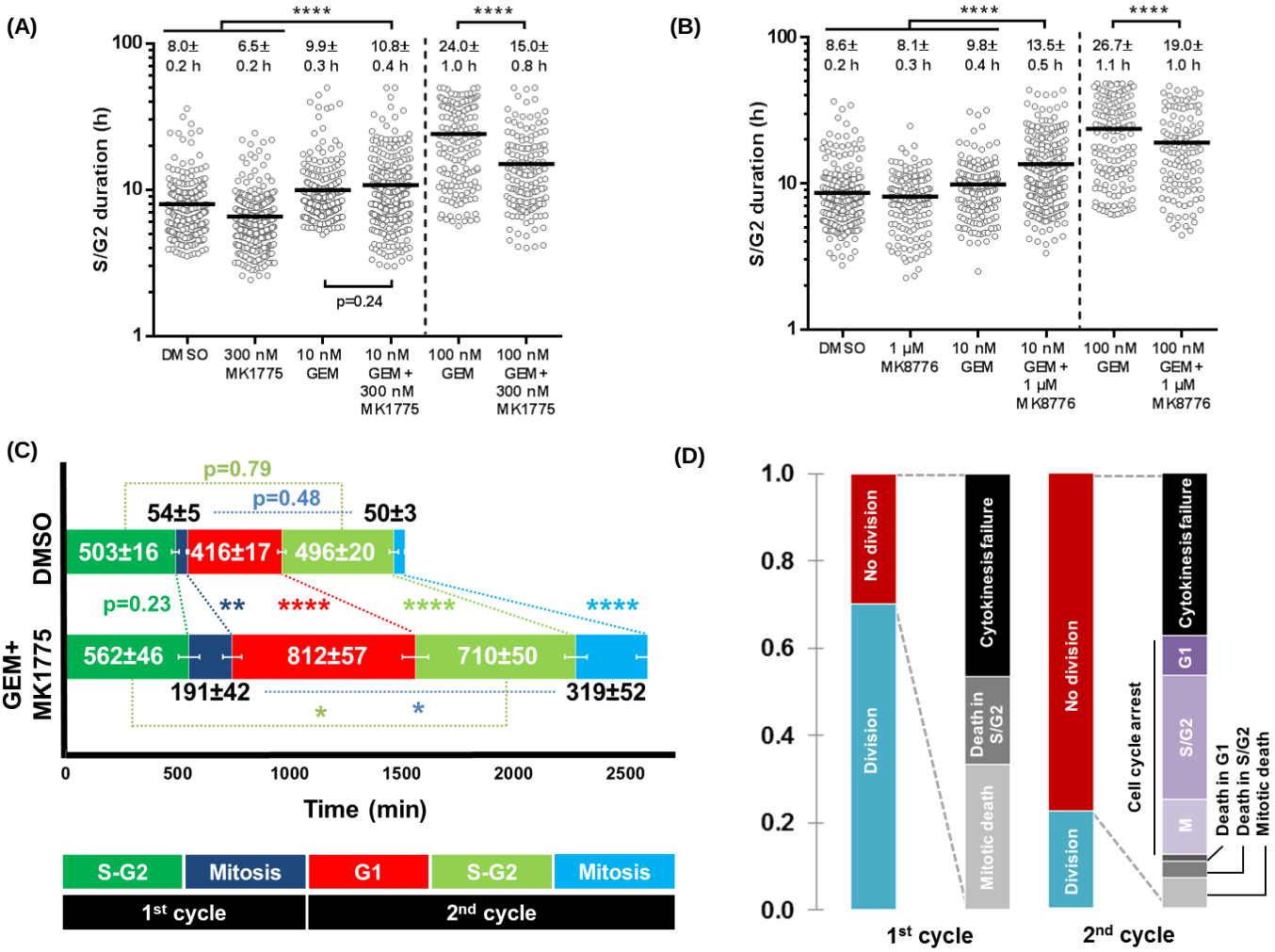
(A)
S/G2 duration (h)
100
10
1
****
****
8.0± 0.2 h
6.5± 0.2 h
9.9± 0.3 h
10.8± 0.4 h
24.0± 1.0 h
15.0± 0.8 h
p=0.24
DMSO
300 nM MK1775
10 nM GEM
10 nM GEM + 300 nM MK1775
100 nM GEM
100 nM GEM + 300 nM MK1775
(B)
S/G2 duration (h)
100
10
1
****
****
8.6± 0.2 h
8.1± 0.3 h
9.8± 0.4 h
13.5± 0.5 h
26.7± 1.1 h
19.0± 1.0 h
DMSO
1 µM MK8776
10 nM GEM
10 nM GEM + 1 µM MK8776
100 nM GEM
100 nM GEM + 1 µM MK8776
(C)
DMSO
GEM+ MK1775
p=0.79
p=0.48
54±5
50±3
503±16
416±17
496±20
p=0.23
**
****
****
****
562±46
812±57
710±50
191±42
319±52
*
*
0
500
1000
1500
2000
2500
Time (min)
S-G2
Mitosis
G1
S-G2
Mitosis
1st cycle
2nd cycle
(D)
1.0
0.8
0.6
0.4
0.2
0.0
No division
Division
Cytokinesis failure
Death in S/G2
Mitotic death
No division
Division
Cell cycle arrest
Cytokinesis failure
G1
S/G2
M
Death in G1
Death in S/G2
Mitotic death
1st cycle
2nd cycle

Figure 3

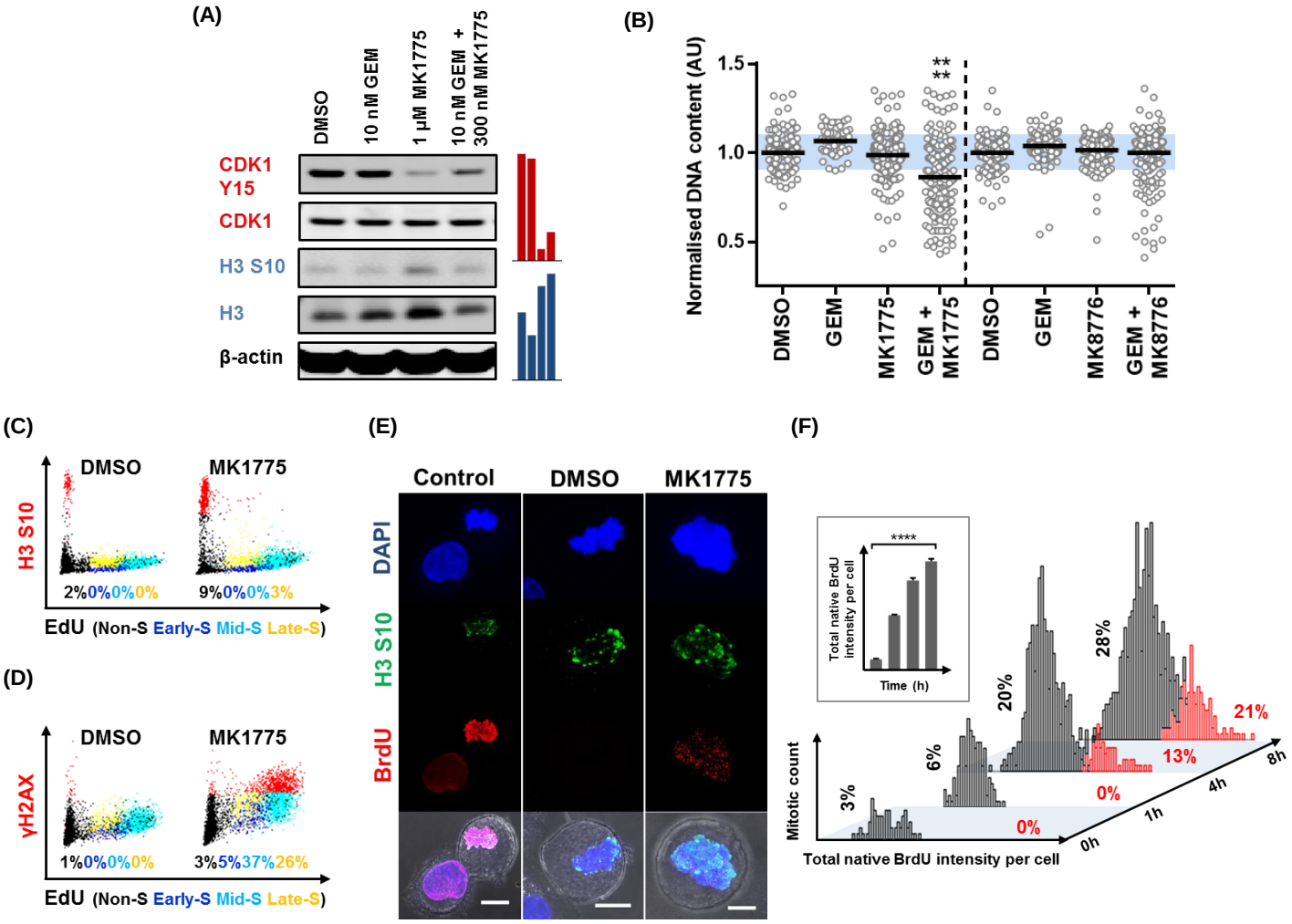
(A)
DMSO
10 nM GEM
1 μM MK1775
10 nM GEM + 300 nM MK1775
CDK1 Y15
CDK1
H3 S10
H3
β-actin
(B)
Normalised DNA content (AU)
1.5
1.0
0.5
**
**
DMSO
GEM
MK1775
GEM + MK1775
DMSO
GEM
MK8776
GEM + MK8776
(C)
DMSO
MK1775
H3 S10
2%0%0%0%
9%0%0%3%
EdU (Non-S Early-S Mid-S Late-S)
(D)
DMSO
MK1775
γH2AX
1%0%0%0%
3%5%37%26%
EdU (Non-S Early-S Mid-S Late-S)
(E)
Control
DMSO
MK1775
DAPI
H3 S10
BrdU
(F)
****
Total native BrdU intensity per cell
Time (h)
Mitotic count
3%
6%
20%
28%
21%
13%
0%
0%
0h
1h
4h
8h
Total native BrdU intensity per cell

Figure 4

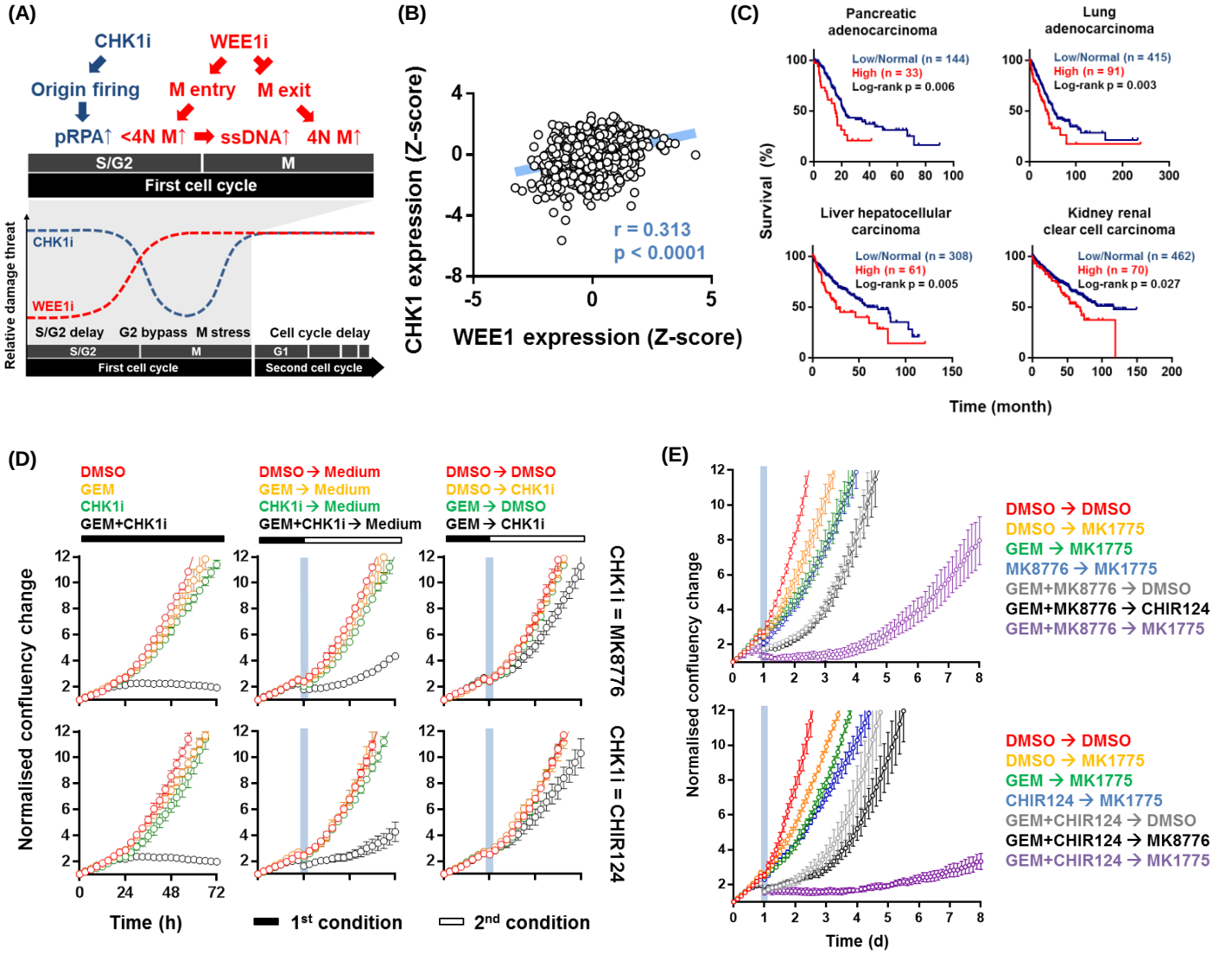
(A)
CHK1i
WEE1i
Origin firing
M entry
M exit
pRPA↑ <4N M↑ ➡ ssDNA↑ 4N M↑
S/G2
M
First cell cycle
CHK1i
WEE1i
Relative damage threat
S/G2 delay
G2 bypass
M stress
Cell cycle delay
S/G2
M
G1
First cell cycle
Second cell cycle
(B)
CHK1 expression (Z-score)
WEE1 expression (Z-score)
r = 0.313
p < 0.0001
(C)
Pancreatic adenocarcinoma
Low/Normal (n = 144)
High (n = 33)
Log-rank p = 0.006
Lung adenocarcinoma
Low/Normal (n = 415)
High (n = 91)
Log-rank p = 0.003
Liver hepatocellular carcinoma
Low/Normal (n = 308)
High (n = 61)
Log-rank p = 0.005
Kidney renal clear cell carcinoma
Low/Normal (n = 462)
High (n = 70)
Log-rank p = 0.027
Survival (%)
Time (month)
(D)
DMSO
GEM
CHK1i
GEM+CHK1i
DMSO → Medium
GEM → Medium
CHK1i → Medium
GEM+CHK1i → Medium
DMSO → DMSO
DMSO → CHK1i
GEM → DMSO
GEM → CHK1i
CHK1i = MK8776
CHK1i = CHIR124
Normalised confluency change
Time (h)
1st condition
2nd condition
(E)
DMSO → DMSO
DMSO → MK1775
GEM → MK1775
MK8776 → MK1775
GEM+MK8776 → DMSO
GEM+MK8776 → CHIR124
GEM+MK8776 → MK1775
DMSO → DMSO
DMSO → MK1775
GEM → MK1775
CHIR124 → MK1775
GEM+CHIR124 → DMSO
GEM+CHIR124 → MK8776
GEM+CHIR124 → MK1775
Normalised confluency change
Time (d)

Figure 5

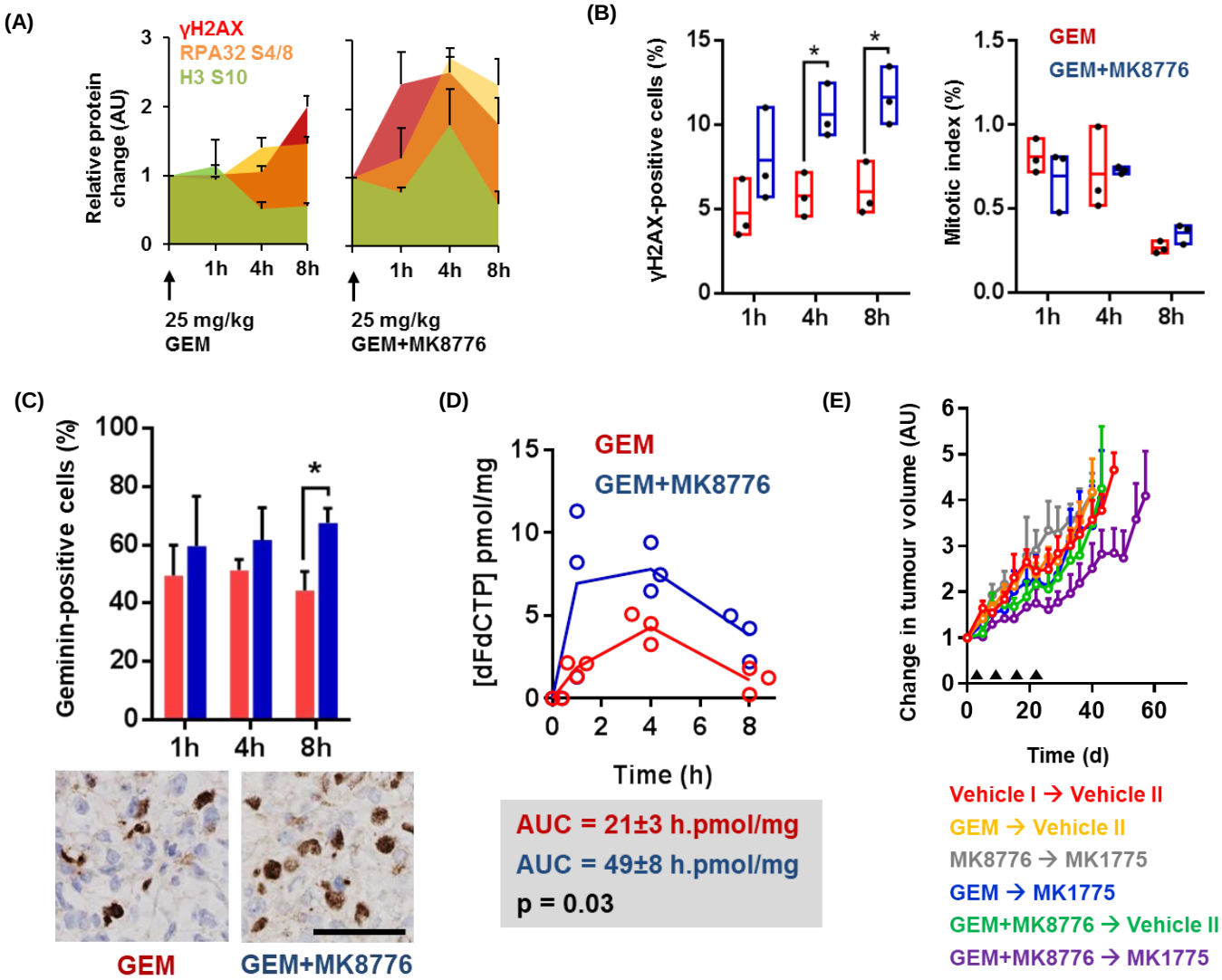
(A)
γH2AX
RPA32 S4/8
H3 S10
Relative protein change (AU)
1h 4h 8h
25 mg/kg GEM
25 mg/kg GEM+MK8776
(B)
γH2AX-positive cells (%)
Mitotic index (%)
GEM
GEM+MK8776
(C)
Geminin-positive cells (%)
GEM
GEM+MK8776
(D)
[dFdCTP] pmol/mg
Time (h)
AUC = 21±3 h.pmol/mg
AUC = 49±8 h.pmol/mg
p = 0.03
(E)
Change in tumour volume (AU)
Time (d)
Vehicle I → Vehicle II
GEM → Vehicle II
MK8776 → MK1775
GEM → MK1775
GEM+MK8776 → Vehicle II
GEM+MK8776 → MK1775

Figure 6

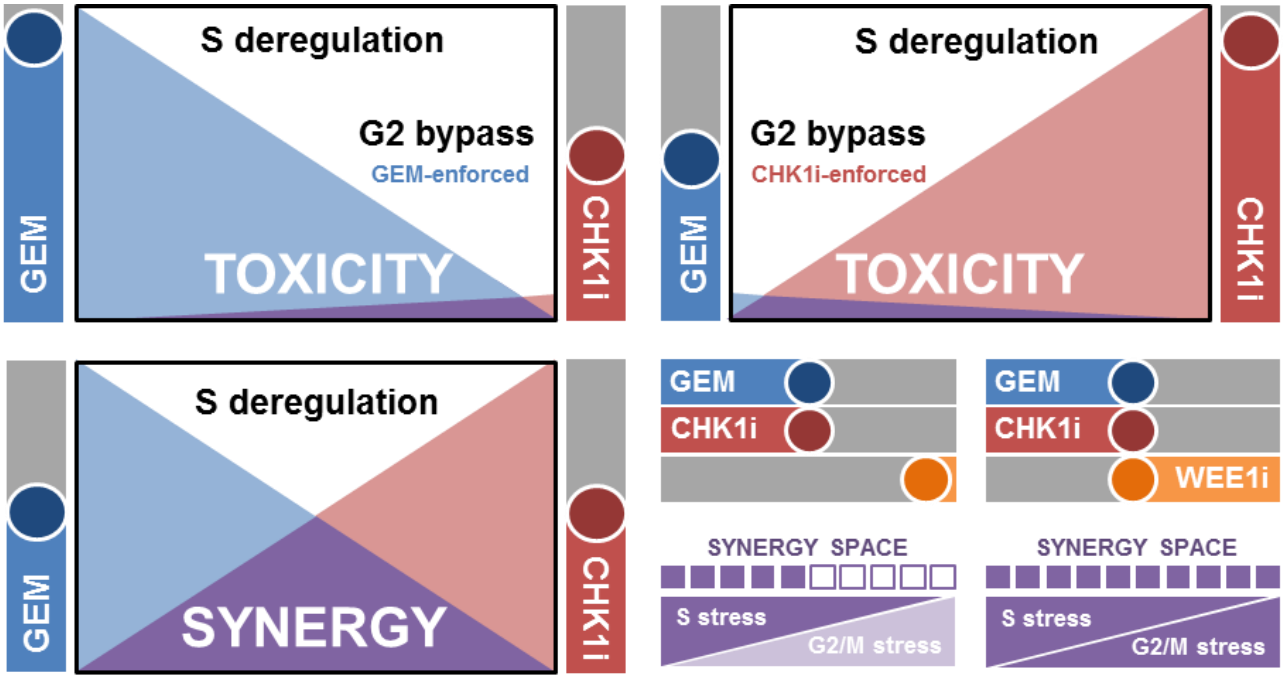
S deregulation
G2 bypass
GEM-enforced
TOXICITY
GEM
CHK1i
S deregulation
G2 bypass
CHK1i-enforced
TOXICITY
GEM
CHK1i
S deregulation
SYNERGY
GEM
CHK1i
GEM
CHK1i
SYNERGY SPACE
S stress
G2/M stress
GEM
CHK1i
WEE1i
SYNERGY SPACE
S stress
G2/M stress